Boosting selective hydrogenation of α,β-unsaturated aldehydes through constructing independent Pt and Fe active sites on support

Yu Liang [a], Jieting He [a], Yurong An [b], Jiaxing Zhang [a], Gyeong-Su Park [d], Liang Zhao [e], Rena Oh [c,*], Xiaoyang Huang [e], Jinxiang Dong [a], Lei Liu [a,*]

[a] Shanxi Key Laboratory of Chemical Product Engineering, College of Chemical Engineering and Technology, Taiyuan University of Technology, Taiyuan 030024, China
[b] School of Physics and Information Technology, Shaanxi Normal University, Xi'an 710119, PR China
[c] Department of Materials Science and Engineering and Research Institute of Advanced Materials, Seoul National University, Seoul, 08826, Republic of Korea
[d] Institute of Next-Generation Semiconductor Convergence Technology, Daegu Gyeongbuk Institute of Science and Technology (DGIST), Daegu 42988, Republic of Korea
[e] Cardiff Catalysis Institute, School of Chemistry, Cardiff University, Main Building, Cardiff CF10 3AT, U.K

ARTICLE INFO

Keywords:
Cooperative catalysis
Adsorptive dissociation
Aldehydes hydrogenation
Hydrogen spillover
Spatial separation

ABSTRACT

The alloy catalysts usually exhibited excellent catalytic synergy owing to the electronic and ensemble effect. However, the process of alloying makes the displacement of the d-band center from the Fermi level, decreasing the adsorption strength of reactant molecules. Herein, we constructed the spatial separation catalyst in which the independent Pt and FeO_x nanoparticles were uniformly distributed on SBA-15 support (denoted as Pt = Fe/SBA-15), which exhibits remarkable efficiency in the hydrogenation of α,β-unsaturated aldehydes, i.e. with a 4 fold higher than the corresponding alloy catalyst in reaction rate, and a 4 fold increase in selectivity for cinnamalcohol production compared to the single Pt catalyst. It is found that Pt primarily catalyzes the H_2 dissociative adsorption into H*, while FeO_x mainly catalyzes the reaction between H* and aldehydes, forming alcohols. Assuming that the rate-determining-step is the H-spillover from Pt to Fe, the two cascade reactions are interconnected. To confirm this mechanism, we employ a physical mixture catalyst of Pt/SBA-15 and FeO_x/SBA-15, where its catalytic activity lies between Pt = Fe/SBA-15 and alloy materials. The catalysts' structures are well characterized by STEM and EDS mapping analysis, and the mechanism is supported by experimental data and DFT calculations. The research we conducted offers a new perspective into the cooperative catalysis, achieved by coupling independent active centers in thermos-hydrogenation reactions.

1. Introduction

The hydrogenation of α,β-unsaturated aldehydes is a crucial industrial reaction [1,2]. The corresponding alcohols can be used in pharmaceutical synthesis, perfume manufacturing, and as spices in food science [3–5]. These valued-added and widely applied products make the reaction process significant. Researchers have discovered that Pt catalysts can be very reactive for this reaction thanks to its high activity in H_2 adsorptive dissociation [6–9]. However, the hydrogenation step of α,β-unsaturated aldehydes over the Pt surface could occur at both theα site (C = O bond) to generate β-unsaturated alcohol and β site (C = C bond) to generate hydrocinnamaldehyde. This presents a challenge in controlling selectivity over C = O bond activation, as exemplified by cinnamaldehyde hydrogenation, which is a significant type of reaction with modern commercial applications (Scheme 1) [10–12]. Thereafter, it was reported that Pt-based alloyed catalysts, i.e., Pt-Co and Pt-Fe, with the d-band center of Pt atoms shifted away from the Fermi level, can reduce the di-σ metal C–C binding energy, resulting in high selectivity for cinnamalcohol [13–16]. Therefore, designing a reactive catalyst through an alloyed structure becomes the key to investigate the utilization of cinnamaldehyde hydrogenation. However, the alloying preparation for Pt-based bimetallic catalysts has also exhibited its limitation. Specifically, the orbital hybridization results in a decrease in the binding energy of di-σ metal C–O over the Pt atoms, leading to a lower reaction rate of cinnamaldehyde hydrogenation compared to the single Pt catalyst [14]. Thus, the imbalance between reactivity and selectivity over the Pt-based alloyed catalysts can be a limiting factor [17].

Recently, Hutchings' group reported that by separating the Au and Pd nanoparticles, the catalysis can be enhanced compared to the Au-Pd alloyed catalyst in alcohol oxidation [18]. This is due to the imbalance

* Corresponding authors.
E-mail addresses: orn415@snu.ac.kr (R. Oh), liulei@tyut.edu.cn (L. Liu).

between oxidative dehydrogenation (ODH) of alcohol molecules and the oxygen reduction reaction (ORR) occurring over the surface of alloyed Au-Pd nanoparticles [19,20]. The simultaneous achievement of maximum activities in the ODH (Oxidative Dehydrogenation) and ORR (Oxygen Reduction Reaction) is hindered by the alloying effect. This effect causes the d-band center to shift away from the Fermi level of Au atoms, resulting in a diminished activity for the dehydrogenation of hydroxyl functional groups in alcohols(C–OH) [21]. Accordingly, in our study, we prepared separated Pt and Fe nanoparticles deposited on SBA- 15 support (denoted as Pt = Fe/SBA-15, weight ratio of Pt:Fe = 1:1) and applied it as a catalyst in cinnamaldehyde hydrogenation. We found that its efficiency surpasses that of the corresponding alloyed Pt-Fe and single Pt catalysts, achieving a 4 fold increase in reaction rate compared to the Pt-Fe alloy, and a 4 fold enhancement in the selectivity towards cinnamalcohol compared to the individual Pt catalyst. As such, this addresses the imbalance between C = O and C-C bonding configurations.

Moreover, we establish that this improvement is due to the coupling of H_2 dissociation and cinnamaldehyde hydrogenation occurring at isolated Pt site and FeO_x sites [22,23]. The H* species dissociated from H_2 molecule can be transferred from the Pt site to the Fe site to complete the catalytic cycle [24]. All the results were supported by STEM, EDS and in-situ DRIFTS, and the mechanism is also corroborated by DFT calculations. Our findings extend the emerging approach of phase-separated catalysis to the creation of multicomponent heterogeneous catalysts for the selective hydrogenation reactions.

2. Experimental section

2.1. Catalyst preparation

FeO_x/SBA-15, Pt/SBA-15 and PtFe/SBA-15 catalysts were synthesized by sol-immobilization. The metal precursors, H_2PtCl_6 and/or Fe $(NO_3)_3$, were added to 100 mL of water and mixed violently. Following that, Polyvinyl alcohol (PVA) was introduced into the solution (mass of PVA / metal = 1.2). A freshly prepared solution of $NaBH_4$ (molar ratio of $NaBH_4$ / metal = 4) was promptly added to the solution, resulting in the formation of a sol. Subsequently, the support material was introduced into the colloidal solution while stirring, which facilitates the immobilization of the metal nanoparticles. Following a 30 min period, the solid catalyst was retrieved by the process of filtration and subsequently rinsed with deinonized water. Ultimately, the catalysts were subjected to a drying process at a 110 °C for 16 h. The Pt = Fe/SBA-15 catalyst is synthesized using sol-immobilization and a two-step sequential reduction process. The synthesis of this material follows a procedure similar to the one described in the previous section. Briefly, the initial step involves preparing the Pt/SBA-15 catalyst as the mother catalyst. Subsequently, the FeO_x is immobilized onto it, resulting in the labeled catalyst of Pt = Fe/SBA-15.

2.2. Catalytic selective hydrogenation

In a typical run, cinnamaldehyde (25 mmol), catalyst (20 mg), and ethanol (5 mL) were introduced into a 25 mL stainless-steel autoclave fitted with a magnetic stirrer. The reaction system is purged with hydrogen (1.0 MPa) and finally to 3.0 MPa, the catalytic hydrogenation of cinnamaldehyde was performed at room temperature for the desired time under stirring at 500 rpm. The products analysis is carried out by Gas Chromatography (GC) (Shimadzu 2010 pro equipped with FID detector and DB-5-HT capillary column).

The Vienna ab initio simulation package (VASP) was used to execute the theoretical calculations. The details of the DFT calculations, characterization, and estimation of catalysts' activation energy are all given in the supplementary data.

3. Results and discussion

3.1. Structural characterization of catalysts

Monometallic Pt, FeO_x, and bimetallic Pt-Fe-based catalysts were synthesized using sol–gel immobilization and supported on SBA-15. Table S1 presented the main physicochemical parameters of SBA-15, both before and after the introduction of metal species, exhibiting almost unchanged surface area and pore size. The content of Pt and Fe, as determined by ICP-AES, was close to 0.2 wt%. TEM/STEM analysis was conducted to examine the morphology and structure of Pt-Fe-bimetallic catalysts, specifically PtFe/SBA-15 and Pt = Fe/SBA-15 catalysts. In Fig. 1, we can find that the SBA-15 support maintains an ordered mesoporous structure after metal loading over catalysts, and the metal (or metal oxide) particles are well dispersed on the support material. TEM images and particle size histograms confirm that Pt nanoparticles (averaging around 2.1 nm) and FeO_x nanoparticles (averaging around 2.9 nm) are very small and distributed uniformly over the SBA-15 support (Fig. 1**a, b**). The effective control of particle size was credited to the introduction of PVA during the synthesis of the nanoparticles, and the spatial segregation of micelles in solution which effectively controlled the nucleation and aggregation of the metal species [25]. Meanwhile, the Pt = Fe/SBA-15 catalyst exhibited a separation between Pt and FeO_x species, where two nanoparticles show respectively different crystal planes with the lattice spacing of 0.226 and 0.270 nm, assigned to (111) plane of Pt *face centered cubic* (space group: Fm-3 m) and (104) plane of α-Fe_2O_3 *trigonal* (space group: R-3c) in Fig. 1**e, f**. Furthermore, HAADF-STEM image (Fig. 1**g**) and EDS maps (Fig. 1**g**–j) for Pt = Fe/SBA-15 catalyst show that the Pt and FeO_x nanoparticles are spatially separated together with their small overlaps on SBA-15 support forming a Janus analogy structure (not alloyed), which is consistent with the STEM (c) and TEM (e) data. Based on the EDS spectrum of the Pt = Fe/SBA-15 catalysts (**Fig. S1** in Supporting Information) with the

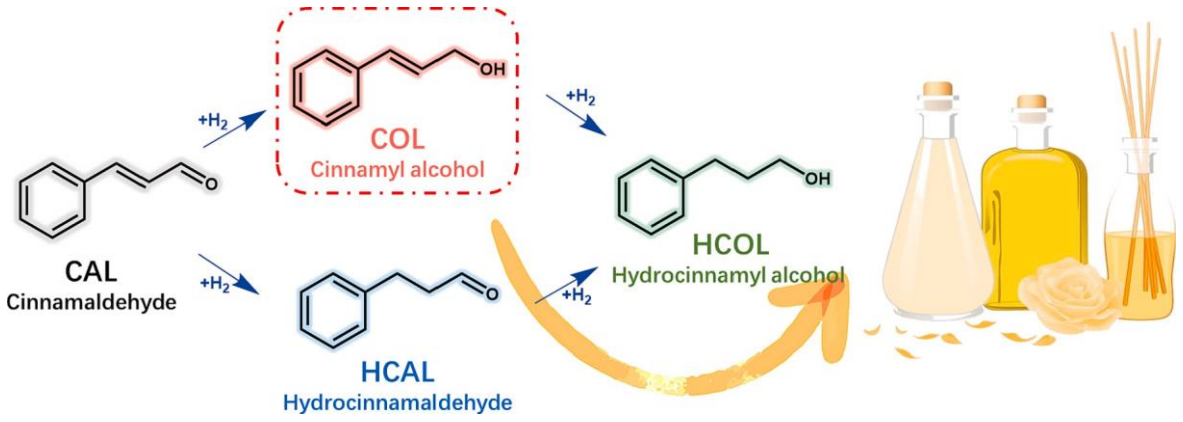

Scheme 1. Typical reaction route for the cinnamaldehyde hydrogenation and its industrial application to essence production.

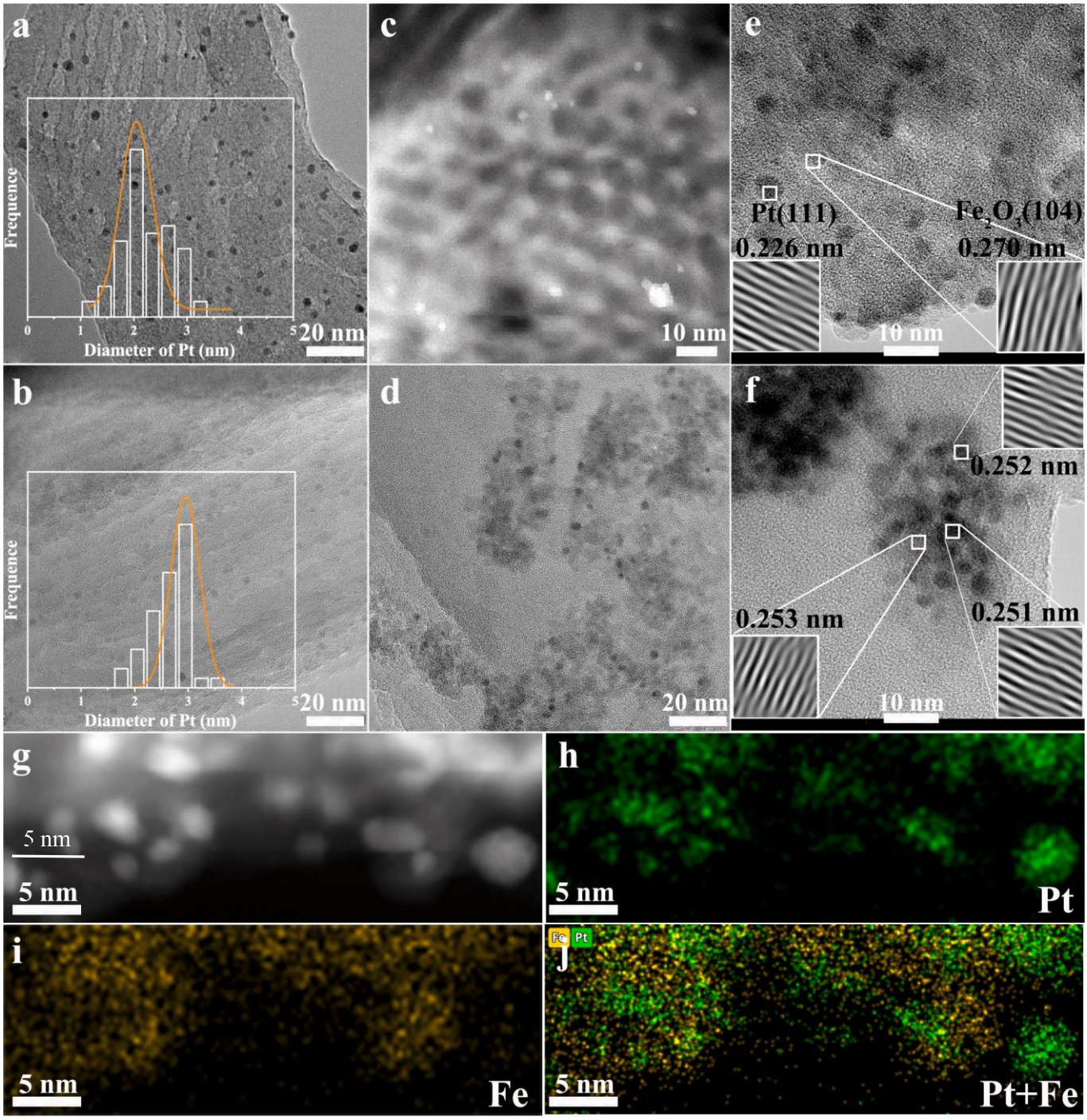

Fig. 1. TEM/STEM images of Pt/SBA-15 (a), FeO_x/SBA-15 (b), Pt = Fe/SBA-15 (c, e), and PtFe/SBA-15 (d, f) catalysts. HAADF-STEM image (g) and EDS maps of Pt (h), Fe (i), and Pt + Fe (j), revealing that Pt and FeO_x particles are spatially separated.

atomic fraction of Pt and Fe on the catalyst surface, the weight ratio of Pt and Fe was calculated to be 1, which is good agreement with that obtained from the ICP test results, further indicating that the Pt and Fe species were uniformly dispersed on the support. On the contrary, the PtFe/SBA-15 catalyst shows a lattice spacing of ~ 0.252 nm, indicating the existence of the PtFe alloy phase as a result of reduction reaction during sample preparation.

To investigate the distribution of Pt and FeO_x species and the stability of SBA-15 supports, XRD patterns of each Pt-Fe-based catalyst and the bare support were analyzed (Fig. 2**a**). The diffraction reflections appeared crystal planes at 2θ of 0.967° (100), 1.641° (110) and 1.865° (200) respectively, were attributed to the long-range mesoporous structure, and corresponded to the P6mm hexagonal structure of the SBA-15 [26]. Due to the low metal loadings, the XRD patterns did not reveal the presence of Pt and FeOx species reflections in the catalysts (Fig. 2**b**). The N_2 adsorption–desorption experiments further confirmed the mesoporous structure of the support material in catalysts. Fig. 2**c and d** exhibited N_2-adsorption–desorption isotherms of IV-type with H_1 hysteresis loops and pore size distribution curves of the mesoporous materials, which were consistent with the commercial SBA-15 support [27]. The average pore sizes of the prepared samples obtained by the BJH method were in a range of 10.2–10.8 nm, which is consistent with

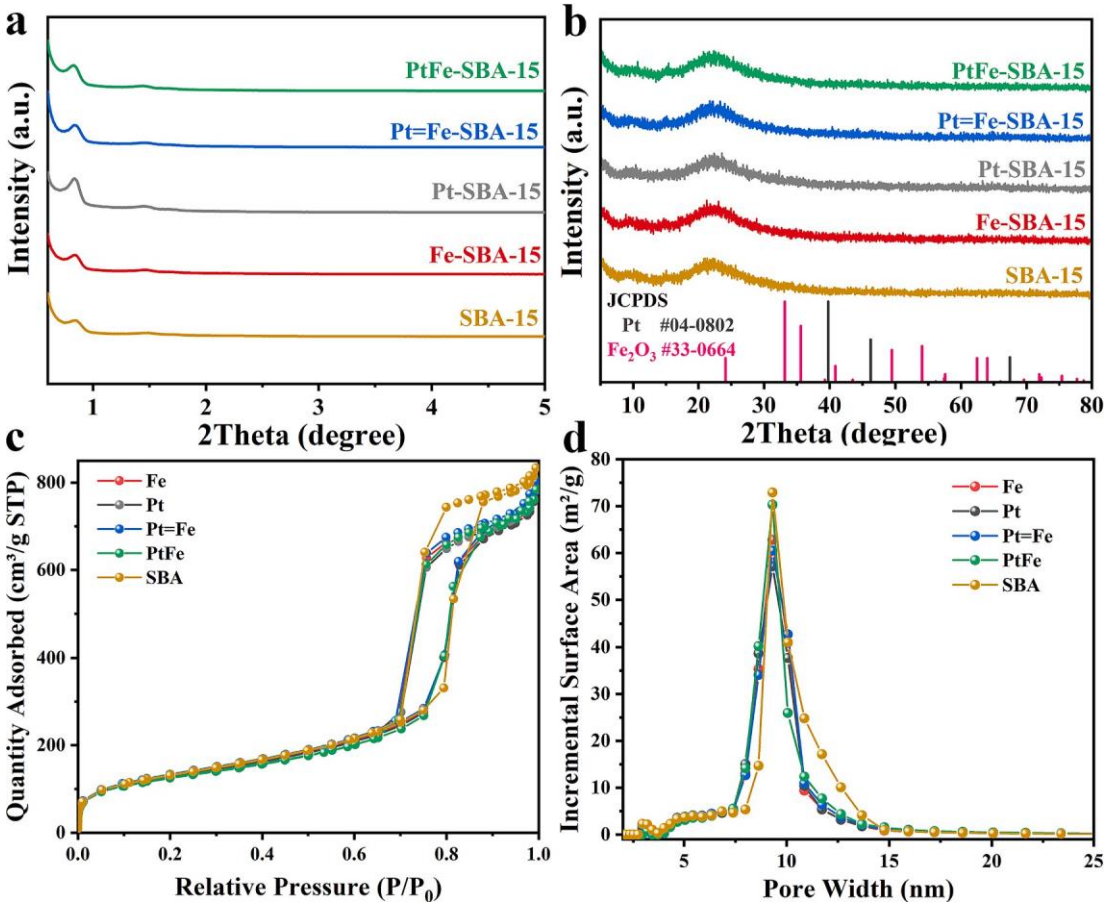

Fig. 2. Powder XRD patterns (a, b) and N_2 adsorption–desorption isotherms (c, d) of the supported Pt and/or FeO_x catalysts on SBA-15 as well as the pristine SBA-15.

the typical mesoporous structure observed in pure SBA-15 [28]. Table S1 summarizes all of these results, demonstrating that the structure of the catalysts remained stable during the preparation, and the Pt and Fe species were deposited on the support surface with a high degree of dispersion.

XPS was operated to further study the electronic structure over the surface of monometallic Pt and bimetallic Pt-Fe catalysts. In Fig. 3**a and** S2, the binding energy at 71.5 and 74.8 eV in pristine Pt 4f are ascribed to Pt^0 $4f_{7/2}$ and $4f_{5/2}$, respectively [29]. Similarly, the Pt 4f binding energy in Pt = Fe/SBA-15 catalyst shows comparable number to that of the Pt/SBA-15, indicating the electronic interaction is very weak be- tween Pt and Fe over the surface of SBA-15. Same case to Fe 2p characterization by XPS, showing the existence of same Fe species in both Pt = Fe/SBA-15 and FeO_x/SBA-15 catalysts (**Fig. S3**). However, the binding energy of Pt $4f_{7/2}$ peak shifts to a low value of 70.9 eV, and Fe 2p peak shifts to higher value in the alloyed PtFe/SBA-15 due to the electron donation from FeO_x to Pt [30], in accordance with the formation of Pt — Fe coordination, and electron transfer occurs in PtFe nanoparticles. This indicates an enhanced electronegativity of $Pt^{\delta-}$ in PtFe/SBA-15.

Besides, we have also characterized the Pt and Fe species' properties by CO-TPD. In Fig. 3**b**, bare SBA-15 support shows an almost flat intensity associated with CO desorption, indicating its weak interaction with CO bond. With the introduction of FeO_x or Pt in SBA-15 as a monometallic catalyst, the signals for CO desorption become apparent (1.19 mmol/g, 1.26 mmol/g respectively), though FeO_x displayed a wider desorption temperature window. Regarding the bimetallic catalyst, the CO desorption peak becomes higher than monometallic Pt and FeO_x catalyst due to CO molecules adsorb on both metals [31]. Specifically, the PtFe/SBA-15 catalyst exhibited a higher CO desorption capacity (1.67 mmol/g) than the Pt = Fe/SBA-15 catalyst (1.57 mmol/g) possibly due to the enriched metallic Pt^0 species from Pt = Fe/SBA-15, which chemisorb the CO molecules strongly for its largely expanded d orbitals [32]. Furthermore, two peaks were deconvoluted in Pt = Fe/SBA-15 at 285 and 330 °C, assigning to Pt and FeO_x, respectively [33]. This could also be another indication that interaction in Pt = Fe/SBA-15 catalyst is weaker than the alloyed PtFe/SBA-15 catalyst between Pt and FeO_x species.

To have a deeper understanding towards the interaction between FeO_x to Pt in each catalyst, CO molecules serve as a sensitive probe for detecting Pt species. The CO-Pt adsorption sites on the catalyst surface of bimetallic or monometallic Pt-based nanoparticles were obtained by performing the in-situ CO-DRIFTS. In Fig. 3**c and** S4, both Pt/SBA-15 and Pt = Fe/SBA-15 catalysts exhibited a vibrational peak at 2084 cm^{-1}, which was ascribed to the linear adsorption of CO on the Pt metal surface [34]. As is agreed well to the XPS results, this could be an indication that the Pt species within the Pt = Fe/SBA-15 appear independently to the Fe species. Notably, a red shift was detected for the linear adsorption band in the PtFe/SBA-15 catalyst, indicating the presence of SMSI between Fe and Pt species [35].

Hydrogen dissociation over each prepared catalyst was investigated by H_2-TPD profiles. (Fig. 3**d**) The observed desorption peak near 300—320 °C was attributed to chemisorbed hydrogen on the surface of the Pt species [36]. Specifically, both the Pt/SBA-15 and Pt = Fe/SBA-15 catalysts showed similar and relatively low temperatures for hydrogen desorption (304 and 309 °C), indicating their strong abilities for hydrogen adsorption and same structure of Pt between the two catalysts, which approves Pt's excellent activity for hydrogen evolution [37]. In contrast, PtFe/SBA-15 catalyst exhibited relatively higher hydrogen desorption temperature (316 °C) than Pt = Fe/SBA-15 and Pt/SBA-15, suggesting the hydrogen adsorption might be inhibited on the

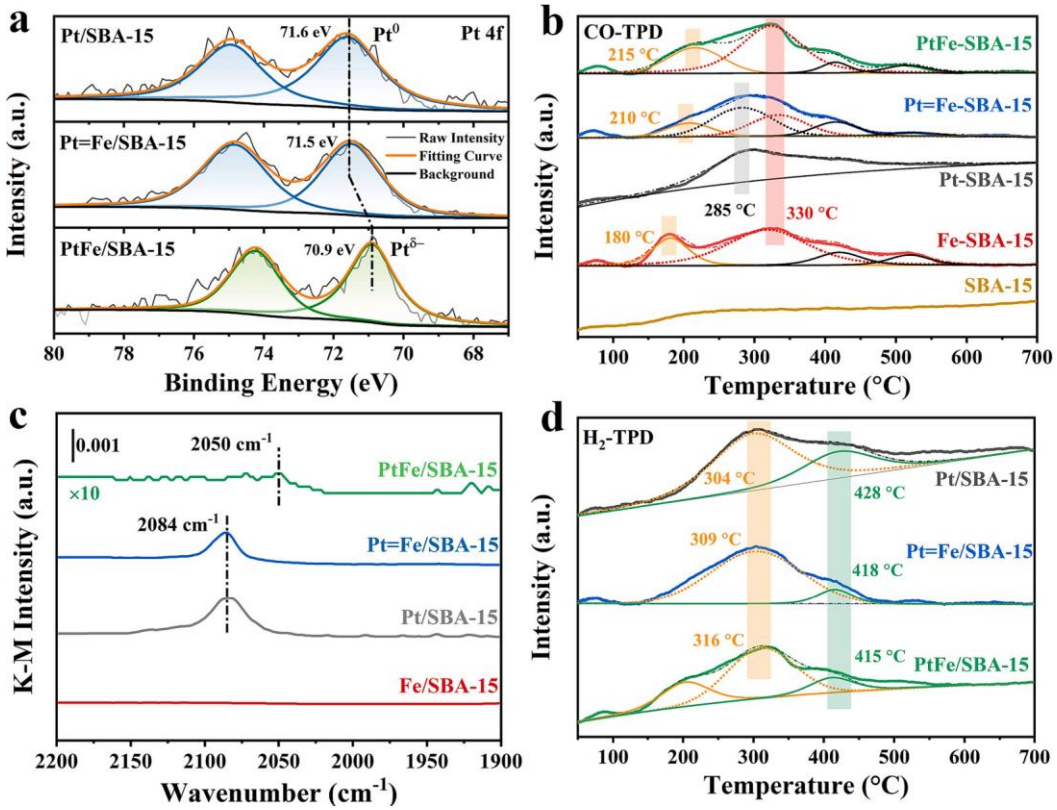

Fig. 3. Catalysts characterization. Pt 4f XPS spectra (a), CO-TPD (b) and In-situ CO-DRIFTS (c) of various Pt/Fe-based catalysts. H_2-TPD profiles (d) of pure SBA-15 and following the introduce of Pt and FeO_x.

catalyst' surface due to the alloyed Fe among Pt atoms [38]. Besides, the tiny desorption peak near over 415 °C was attributed to the hydrogen overflow on the catalyst surface (typically occurred on the surface of reducible metal oxides) [39].

3.2. Catalytic performance in selective hydrogenation

The series of Pt/Fe-based catalysts were investigated for CAL hydrogenation, (a typical molecular of UAL). (Fig. 4**a–c**) CAL conversion and COL (product) selectivity were monitored as a function of time, temperature. While elevating the reaction temperature enhances H_2 dissociation activity over Pt, accounting for the improved CAL hydrogenation activity over monometallic Pt/SBA-15 (Fig. 4**b**), it is essential to note that the rate-limiting step is believed to be the H spillover from Pt to the FeO_x site. Particularly for the physical mixture catalyst, the H spillover process primarily occurs upon contact between Pt/SBA-15 and FeO_x/SBA-15 grains during the reaction. This elucidates why the reaction temperature has a diminished effect on the mixed catalyst. Whilst in the case of the PtFe/SBA-15 catalyst, its activity exhibits a rapid increase with higher reaction temperatures. In our work, the hydrogenation performance is mainly occurred and limited by the adsorption of C = O groups on the FeO_x species (not the noble metal) under excess hydrogen, leading to a relatively stable selectivity towards COL (Fig. 4**d**). The spatially separated active sites (Pt and FeO_x) make a strong synergy, where the Pt is very active mainly in generating H* species from H_2 dissociation. Subsequently, these H* species are supposed to transfer from Pt to the FeO_x site by H-spillover. Therefore, the H spillover among different active sites can be another limiting factor, which further hydrogenates the COL to HCOL. Therefore, less influence was obtained on COL selectivity by hydrogen pressure, limited by its spillover, through separating the metals as two independent active sites for catalyzing two different reactions.

The Pt/SBA-15 catalyst showed a low selectivity (~20 %) during the entire duration of the experiment. Catalytic selectivity towards COL gets immediately increased to ~ 50 % after the addition of Fe/SBA-15 catalyst to form a physical mixture catalyst with Pt/SBA-15. Moreover, the activity of physical mixture catalysts (rate of 1.4×10^{-5} $mol \cdot L^{-1} \cdot s^{-1}$) was far greater than that observed with the bimetallic PtFe/SBA-15 alloy catalyst (rate of 4.4×10^{-6} $mol \cdot L^{-1} \cdot s^{-1}$), which could therefore expect a strong synergistic effect between the two-counterpart catalyst of during reaction. Preliminarily, it was reported that the alloying process will decrease the binding energy of di-σ metal C–O over the surface of Pt atoms, resulting in a lower reaction rate of cinnamaldehyde hydrogenation [14,40]. Whilst, separating the Pt and Fe as two independent natures (not alloyed) in one catalyst, which liberates the two active sites for catalyzing two different reactions, meanwhile coupling the two reactions through reaction intermediates transfer is an alternative strategy to enhance the catalysis. To confirm this, the as prepared Pt = Fe/SBA-15 catalyst with independent active sites of Pt and Fe depositing on the same SBA-15 support was applied for the same reaction, where its performance in terms of reaction rate (rate of 1.6×10^{-5} $mol \cdot L^{-1} \cdot s^{-1}$) and COL selectivity (~90 %) can be further enhanced.

An important factor in comprehending this phenomenon is the adsorption mode in which reactant molecules on the surfaces of Pt and Fe species. Herein, we carried out in-situ DRIFTS measurements to investigate the 3-methy-2-butenal probe molecule bonds to the surface of monometallic Pt, FeO_x, and bimetallic Pt-Fe-based catalysts, respectively. The reaction cell was filled with pure 3-methy-2-butenal at room temperature for a duration of 30 min. However, despite the experimental efforts, the gaseous or physically adsorbed 3-methy-2-butenal was still remained inside the DRIFTS cell when there is no catalyst, as seen in Fig. 4**d**. The bands at 1681 and 1666 cm^{-1} are assigned to ν(C═O) and ν(C═C) stretching of aldehyde, respectively [41]. Notably, when using the Pt/SBA-15 catalyst, the intensity of the ν(C═C) peak significantly decreased, and a new peak emerged at 1674 cm^{-1}. This

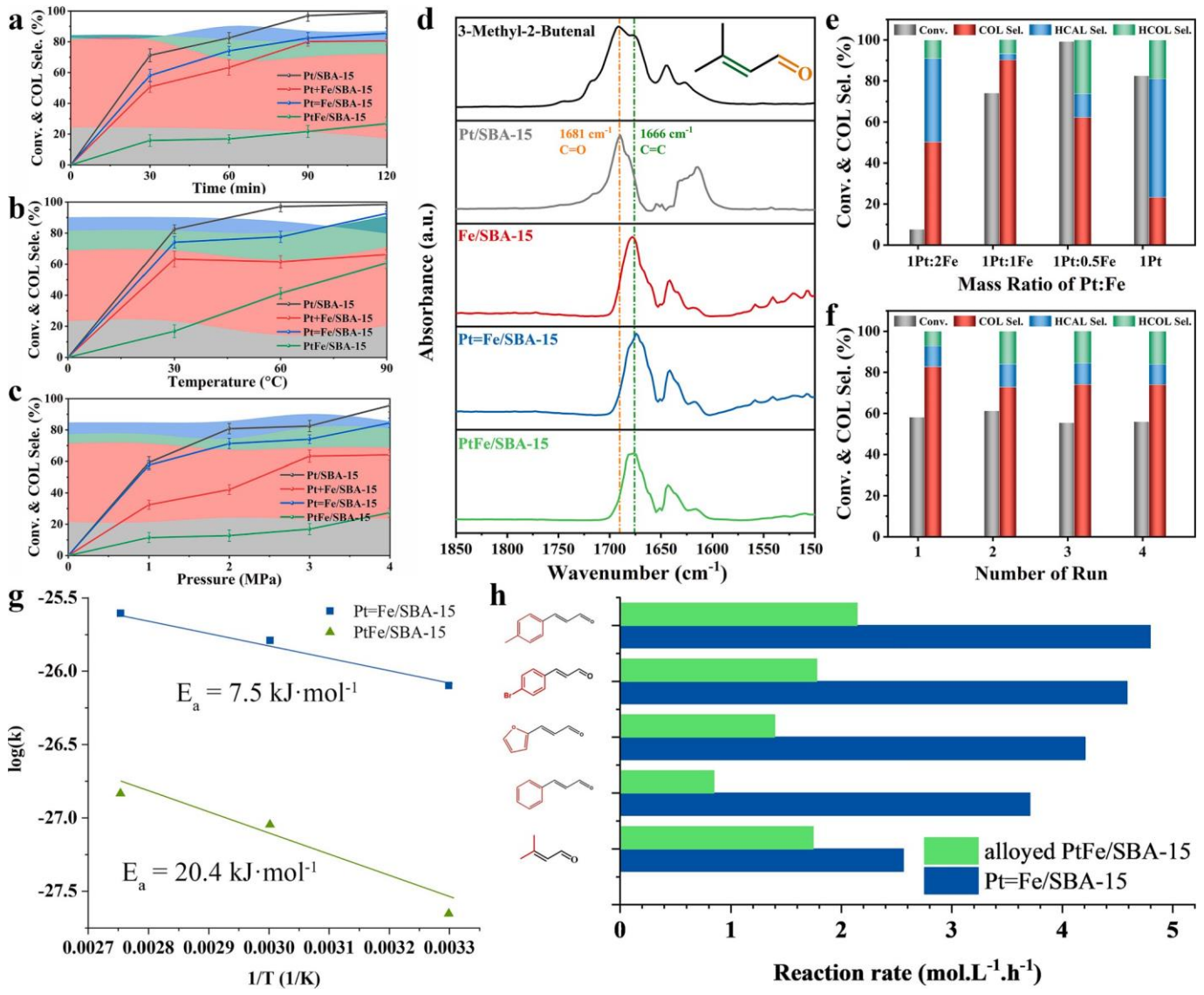

Fig. 4. The CAL hydrogenation performance over catalysts at various reaction conditions. {Time (a), Temperature (b), and Pressure (c)} (d) In-situ DRIFTS of 3-methyl-2-butenal adsorbed on monometallic Pt, FeO_x and a bimetallic Pt-Fe based catalysts. (e) Catalytic results for CAL hydrogenation over Pt = Fe/SBA-15 catalysts at various mass ratio of Pt: Fe. (f) Reusability of Pt = Fe/SBA-15 catalyst for the CAL hydrogenation (Reaction conditions: 25 mmol CAL, 0.02 g catalyst, 3.0 MPa initial H_2 pressure, 5 mL EA, and room temperature). (g) Thermo activation energy of PtFe/SBA-15 and Pt = Fe/SBA-15 catalysts in CAL hydrogenation reaction. (h) Comparison of reaction rate between the PtFe/SBA-15 and Pt = Fe/SBA-15 catalysts over a series of hydrogenation reaction of α,β-unsaturated aldehydes, reaction conditions: 20 mg catalysts; 25 mmol substrate; 5 mL EA; 60 min; 600 rpm; room temperature.

new peak is assumed to be originated from the C = C bond chemically adsorbed onto a Pt surface. Meanwhile, the peak from ν(C═O) did not change, suggesting that adsorptive activation of C = O bond could not occur over Pt/SBA-15 catalyst. It conducts to a low selectivity to COL product (CAL → COL). In contrast, for Fe-based catalysts (Pt = Fe, PtFe, and FeO_x), the peak intensity of ν(C═O) disappeared without major changes in ν(C═C). This suggests that the presence of FeO_x in the catalyst promotes the adsorptive activation of the C═O bond, resulting in a highly active catalyst with a strong preference for COL product. The noticeable difference in adsorptive activation between C═O and C═C suggests the ability to control selectivity towards hydrogenation products. This difference may be attributed to the alteration in the geometric structure of adsorption sites, which will be examined in more detail through DFT calculations.

In order to verify the critical role of the Pt and FeO_x species, hydrogenation over Pt = Fe/SBA-15 catalysts at various mass ratios of Pt: Fe were also performed. (Fig. 4**e**) Among which, the Pt_1 = Fe_1/SBA-15 catalyst exhibited excellent performance to convert CAL to COL (selectivity of 90 %). Raising the Pt: Fe ratio in catalyst increased the CAL conversion while decreasing the COL selectivity, which was attributed to over-hydrogenation arising from the increased Pt-Pt sites. Furthermore, the assess of the Pt = Fe/SBA-15 catalyst's reusability was conducted by performing the reactions using the previously utilized catalyst (Fig. 4**f**). After 4 cycles, it is evident that there is no distinct decrease in CAL conversion, and the selectivity towards COL decreased from 82 % to 73 %. To investigate the reason of COL decrease especially after the first run, the Pt and FeO_x content in the spent catalyst was measured by ICP-AES. (Table S2) It was found that the Fe content had a slight drop from 0.2 % to 0.18 % after first run, but after that the Fe loss could be negligible in the next runs. In the case of Pt species, no obvious weight loss was observed in four successive runs. The loss of Fe in the firs run is probably due to the dissociation of some Fe species in SBA-15 that had a weakly interaction with support under stirring during reaction. The rising ratio of Pt: Fe species causes deep hydrogenation of CAL to HCOL.

This experimental results could account for the fact that the selectivity towards COL decreased from 82 % to 73 % after one cycle, and remained stable in the next runs. ICP-AES analysis of post-reaction solutions confirms that the rate improvement did not occur due to any metal leaching in the reactions. Further calculations on activation energy of Pt = Fe/SBA-15 and PtFe/SBA-15 were determined to be E_a of 7.5 and 20.4 kJ.mol^{-1}, respectively(Fig. 4**g**). Calculation details were provided in the Supplementary Information. The alloying process, serving as the activity centers, diminishes the adsorption of reactant molecules and consequently lowers the reaction rates [42]. Moreover, the absence of structural control impedes further enhancement due to the indiscriminate blocking of Pt active sites by the second metal promoters [43]. Despite the abundance of H_2, the primary factor restricting the reaction rate in our system is the adsorption of C = O groups at the active center of FeO_x. In contrast to the conventional reaction path, employing separate metals as two independent active sites (Pt and FeO_x) for catalyzing two different reactions (hydrogen dissociation and UAL hydrogenation) proves to be an effective method for reducing the activation energy.

Fig. 4**h** displays the catalytic performance of Pt = Fe/SBA-15 and PtFe/SBA-15 catalysts in the hydrogenation of different unsaturated aldehydes, it was observed that the Pt = Fe/SBA-15 catalyst exhibited a greater hydrogenation rate for various substrates compared to the corresponding PtFe/SBA-15. Table S3 and S4 display the products selectivity, showing Pt = Fe/SBA-15 catalyst also present a good selectivity towards the alcoholic product. Therefore, with all substrates, the Pt = Fe/SBA-15 catalyst favors C = O hydrogenation over C = C. For example, α-methyl cinnamaldehyde and 4-methyl cinnamaldehyde, it gives a low selectivity of 68 %, which could be that the polar group leads to the strong adsorption of activity center over reactants [2]. Notably, other unsaturated aldehydes all present > 80 % selectivity to the corresponding unsaturated alcohols.

To further understand the role of SBA-15 support, we performed the hydrogenation of the CAL using homogeneous dispersion Pt, PtFe (alloyed), and Pt + FeO_x sol–gel (physical mixture) as a direct catalyst. Interestingly, once the SBA-15 is absent, it shows a decreased selectivity by using Pt + FeO_x sol–gel compared to the alloyed PtFe toward COL using (**Table S5**), indicating that SBA-15 support can be a good media to facilitate the interaction between Pt and FeO_x during their reaction, perhaps through H-spillover. On this basis, another experiment was conducted to examine how the choice of solvent influences the control of hydrogen transfer in the reaction. (**Table S6**) Upon changing the solvent from ethanol to isopropanol, the COL selectivity decreases rapidly, which could be attributed to the inability of the transfer of dissociated hydrogen atoms from Pt to FeO_x species, resulting in a decreased CAL conversion and an increased selectivity towards HCAL due to the C = C bond activation [44]. All these results indicate the hydrogenation reaction of CAL can be separated into 1) H_2 dissociation and H-spillover and 2) reaction between H* and CAL, catalyzed by independent Pt and FeO_x active sites, however strongly coupled together in the heterogeneous hydrogenation system especially with ethanol solvent.

So far, we have determined that the Pt = Fe/SBA-15 catalyst exhibits superior catalytic performance compared to the alloyed PtFe/SBA-15 catalyst in CAL hydrogenation (Fig. 5**a**). Afterwards, we performed the DFT calculations to determine the site of hydrogenation and the selectivity based on the adsorbed configuration of the substrate [4]. On the basis of the DFT calculations in Fig. 5**b**, together with the DRIFTS results discussed in Fig. 4**d**, the CAL adsorption mode over the Pt = Fe/SBA-15 catalyst as well as the reaction pathway can be demonstrated. In the optimized complex between a modeled Pt/SBA-15 catalyst and CAL molecule, 6 carbons of the benzene ring of CAL form the bonds to 4Pt atoms with an −3.16 eV adsorption energy. In contrast, in the optimized complex of a simulated Fe_2O_3/SBA-15 and CAL molecule, the Fe atom is bonded to the terminal O atom with an adsorption energy of −0.97 eV. Consequently, the adsorption preference of the FeO_x species over the C = O group in the CAL leads to a high catalytic selectivity for COL [45]. Based on this, the reactant (CAL), catalysts (FeO_x/SBA-15), and ethyl alcohol were charged in the reactor sealed under Ar atomosphere (0.1 MPa) and kept at 200 °C for 10 h. The FeO_x/SBA-15 demonstrated a very high selectivity of 91.5 % towards COL under a CAL conversion of 28 %, suggesting that ethyl alcohol serves as the hydrogen donor in the process. Meanwhile, the significantly high selectivity proves that FeO_x is able to be the adsorption site for C = O groups, see Fig. 5**a** [14]. Given that FeO_x shows less activity in hydrogen dissociation, we had therefore run the reaction at a higher temperature of 200 °C with an increased amount of catalyst during the experiment.

Based on all these observations, we are able to propose a reaction mechanism over Pt = Fe/SBA-15 catalyst for the hydrogenation of CAL with a phase separated structure.

Initially, H_2 molecules adsorb on the Pt site, and dissociate into H atom adsorbates. The generated H* species will then transfer to the FeO_x site by H-spillover. The α-C in the C═O bond is attacked by the active H* on the surface of the FeO_x phase, resulting in the formation of R-CH_2═O* followed by another attack on the O* in the C═O bond, causing the desorption of COL [46,47]. Thanks to the synergistic cooperation between Pt and FeO_x phase (not alloyed), the rate and product selectivity can be enhanced during CAL hydrogenation to COL, see **Equations** below (Eq. 1–5). Finally, for CAL hydrogenation to COL (Table 1), our Pt = Fe/SBA-15 catalyst is the most active among the reported performances so far.

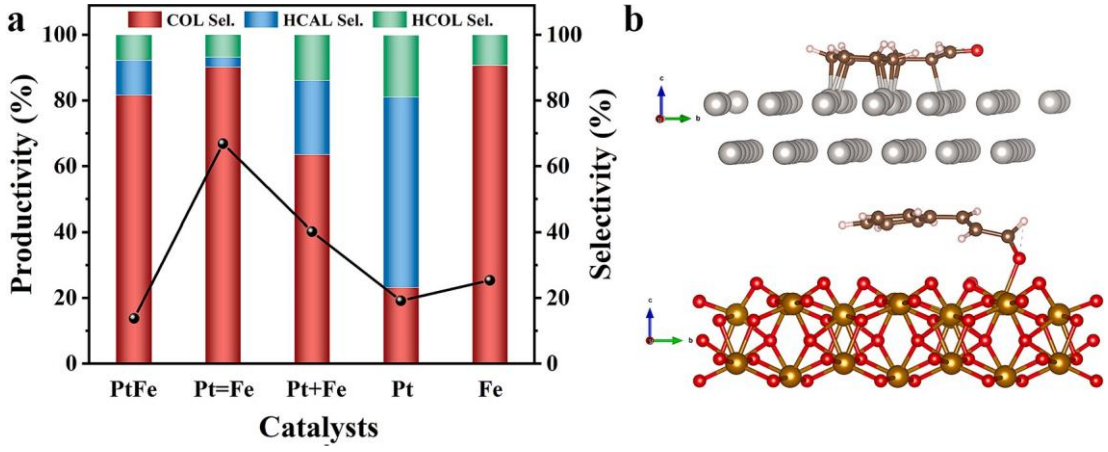

Fig. 5. (a) A comparison of catalytic results over various catalyst for hydrogenation of CAL. Reaction conditions: Pt-based/SBA-15 catalyst 0.02 g; 25 mmol CAL; 3.0 MPa initial H_2 pressure; 5 mL EA; 600 rpm, 60 min, and room temperature. For Fe/SBA-15, 0.06g catalyst, 600 min, and 200 °C were applied for reaction; (b) The optimized geometry of CAL adsorption over Pt and Fe_2O_3 surfaces.

Table 1
The performance of reported the CAL hydrogenation catalysts in literature in terms of reaction temperature, pressure and used catalyst amount.

Catalyst	P (MPa)	T (℃)	CAL (mmol)	Time (h)	Amount (g)	Productivity (mol/g_{cat}/h)	Ref.
Pt = Fe/SBA-15	3	RT	25.00	0.5	0.02	1.183	this work
PtFe/HPZSM-5	2	90	11.25	1	0.025	0.386	[23]
Ni/SBA-15R	2	100	0.55	2	0.05	0.000	[48]
PtFe/CNT	2	60	3.18	1.5	0.01	0.123	[43]
FeCo/NC	2	80	1.00	2	0.02	0.022	[49]
NiP	1.5	70	0.50	5	0.01	0.010	[50]
Ir/C	2	150	158.90	2	1	0.047	[51]
PtFeZn/C	1.6	75	15.89	3	0.3	0.008	[52]
Au/ZnO	2	110	0.20	0.83	0.1	0.002	[53]
Pt/BN	4	25	5.00	2	0.1	0.020	[54]
RuSnB/CeO_2	2	100	1.59	2	0.002	0.150	[55]
Pt-Co/CNTs	2.6	60	8.00	1.5	0.36	0.013	[56]
Pt/SiO_2	2	76	75.67	5	0.19	0.063	[57]
PtFeO_x/TiO_2@SBA-15	4	90	7.50	1	0.05	0.125	[58]
Au/ZnAl	1.5	130	0.25	5	0.05	0.001	[59]
Ru@ZnO/CN	Ambient	140	0.50	6	0.02	0.003	[60]

$$H_2 \xrightarrow{Pt\ site} H^* + H^* \quad (1)$$

$$R\text{-}CH=O \xrightarrow{FeO_x\ site} R\text{-}CH=O^*(adsorption) \quad (2)$$

$$H\text{-}spillover \quad (Pt\ site \rightarrow FeO_x\ site) \quad (3)$$

$$R\text{-}CH=O^* + 2H^* \rightarrow R\text{-}CH_2\text{-}OH \quad (4)$$

$$Product\ desorption \quad (5)$$

Therefore, analogous to the 'CORE' works from Hutchings group, for multicomponent heterogeneous catalyst, we conclude that by separating the Pt and Fe nanoparticles with a mass ratio of 1:1 as two independent active sites, and depositing on SBA-15 support, it is able to couple hydrogen dissociation reaction and C═O hydrogenation, giving rise to an excellent catalysis performance.

4. Conclusions

Monometallic Pt, FeO_x, and their bimetallic catalysts on SBA-15 support were synthesized through a sol–gel approach. The Pt = Fe/ SBA-15 catalyst demonstrates a significantly improved behavior for the CAL hydrogenation to COL, which is six times higher in terms of productivity than the alloyed PtFe/SBA-15 catalyst. In the Pt = Fe/SBA-15, we propose a cooperative catalytic effect stemming from the independent active sites of Pt and FeO_x during the reaction. The CAL molecules undergo adsorptive activation and react with the hydrogen atoms on the FeO_x site. As such, spatially separating the Pt and FeO_x site into two individual active sites over the support material couples two different catalytic reactions through the transfer of the reaction intermediate. We are confident that this approach offers significant potential for multicomponent heterogeneous catalysts. They can function as efficient catalysts for selectively hydrogenating unsaturated carbonyl compounds.

Author Contributions

Y.L., L.L., R.O., and X.Y.H. contributed to the design of the study. J.T. H., J.X.Z, and Y.A. conducted experiments and data analysis. L.Z., and J. X.D. provided technical support, conceptual advice, and result interpretation. R.O., and G-S.P. performed characterizations of materials, including TEM and the corresponding data analysis. Y.L., X.Y.H., L.L., and R.O. wrote the manuscript and supplementary data. All authors commented on and amended both documents. All authors discussed and contributed to the work.

CRediT authorship contribution statement

Yu Liang: Data curation, Formal analysis, Writing – original draft. **Jieting He:** Investigation, Resources. **Yurong An:** Supervision, Validation. **Jiaxing Zhang:** Investigation, Resources. **Gyeong-Su Park:** Funding acquisition, Resources. **Liang Zhao:** Conceptualization, Resources. **Rena Oh:** Resources, Software. **Xiaoyang Huang:** Methodology, Project administration, Writing – review & editing. **Jinxiang Dong:** Methodology, Supervision. **Lei Liu:** Funding acquisition, Project administration, Supervision, Writing – review & editing.

Declaration of competing interest

The authors declare that they have no known competing financial interests or personal relationships that could have appeared to influence the work reported in this paper.

Data availability

Data will be made available on request.

Acknowledgements

The research was financially supported by the National Natural Science Foundation, China (U1910202 and 21978194), the Key Research and Development Program of Shanxi Province, China (202102090301005). X.Y.H. thanks Dr Ouardia Akdim from Cardiff Catalysis Institute for the significant discussion. This research was supported by the National Research Foundation of Korea, South Korea (NRF) funded by the Ministry of Science, ICT & Future Planning (NRF-2021R1A2C1011046).

Appendix A. Supplementary data

Supplementary data to this article can be found online at https://doi.org/10.1016/j.cej.2024.149670.

References

[1] M. Luneau, J.S. Lim, D.A. Patel, E.C.H. Sykes, C.M. Friend, P. Sautet, Guidelines to achieving high selectivity for the hydrogenation of α, β-unsaturated aldehydes with bimetallic and dilute alloy catalysts: a review, Chem. Rev. 120 (23) (2020) 12834–12872.
[2] X. Lan, T. Wang, Highly selective catalysts for the hydrogenation of unsaturated aldehydes: a review, ACS Catal. 10 (4) (2020) 2764–2790.
[3] Q. Liu, Q. Liu, Y. Chen, Y. Li, H. Su, Q. Liu, G. Li, Ir nanoclusters confined within hollow MIL-101 (Fe) for selective hydrogenation of α, β-unsaturated aldehyde, Chinese Chem. Lett. 33 (1) (2022) 374–377.

[4] Y. Liang, Q. Tang, L. Liu, D. Wang, J. Dong, Fabrication of highly oxidized Pt single-atom catalysts to suppress the deep hydrogenation of unsaturated aldehydes, Appl. Catal. B Environ. 333 (2023) 122783.

[5] Q. Liu, Y. Li, Y. Fan, C.-Y. Su, G. Li, Chemoselective hydrogenation of α, β-unsaturated aldehydes over Rh nanoclusters confined in a metal–organic framework, J. Mater. Chem. A 8 (22) (2020) 11442–11447.

[6] Z. Tian, Q. Li, J. Hou, Y. Li, S. Ai, Highly selective hydrogenation of α, β-unsaturated aldehydes by Pt catalysts supported on Fe-based layered double hydroxides and derived mixed metal oxides, Catal. Sci. Technol. 6 (3) (2016) 703–707.

[7] M. Stucchi, F. Vasile, S. Cattaneo, A. Vomeri, A.B. Hungria, L. Prati, Pt-WOx/C catalysts for α, β-unsaturated aldehydes hydrogenation: An NMR study of the effect of the reactant adsorption on activity and selectivity, European J. Org. Chem. 2022 (40) (2022) e202200735.

[8] P.-C. Kang, Y.-S. Ou, G.-L. Li, J.-K. Chang, C.-Y. Wang, Room-temperature hydrogen adsorption via spillover in Pt nanoparticle-decorated UiO-66 nanoparticles: implications for hydrogen storage, ACS Appl. Nano Mater. 4 (10) (2021) 11269–11280.

[9] P. Kuang, Z. Ni, B. Zhu, Y. Lin, J. Yu, Modulating the d-band center enables ultrafine Pt3Fe alloy nanoparticles for pH-universal hydrogen evolution reaction, Adv. Mater. 35 (41) (2023) 2303030.

[10] S. Cattaneo, S.J. Freakley, D.J. Morgan, M. Sankar, N. Dimitratos, G.J. Hutchings, Cinnamaldehyde hydrogenation using Au–Pd catalysts prepared by sol immobilisation, Catal. Sci. Technol. 8 (6) (2018) 1677–1685.

[11] L. Li, Z.-F. Jiao, J.-X. Zhao, D. Yao, X. Li, X.-Y. Guo, Boosting the selectivity of Pt catalysts for cinnamaldehyde hydrogenation to cinnamylalcohol by surface oxidation of SiC support, J. Catal. 425 (2023) 314–321.

[12] K. Yuan, T. Song, D. Wang, X. Zhang, X. Gao, Y. Zou, H. Dong, Z. Tang, W. Hu, Effective and selective catalysts for cinnamaldehyde hydrogenation: Hydrophobic hybrids of metal–organic frameworks, metal nanoparticles, and micro-and mesoporous polymers, Angew. Chemie Int. Ed. 57 (20) (2018) 5708–5713.

[13] Y. Liang, M. Douthwaite, X. Huang, B. Zhao, Q. Tang, L. Liu, J. Dong, Zero-oxidation state precursor assisted fabrication of highly dispersed and stable Pt catalyst for chemoselective hydrogenation of α, β-unsaturated aldehydes, Nano Res. 16 (5) (2023) 6085–6093.

[14] W.O. Oduro, N. Cailuo, K.M.K. Yu, H. Yang, S.C. Tsang, Geometric and electronic effects on hydrogenation of cinnamaldehyde over unsupported Pt-based nanocrystals, Phys. Chem. Chem. Phys. 13 (7) (2011) 2590–2602.

[15] Q. Zheng, D. Wang, F. Yuan, Q. Han, Y. Dong, Y. Liu, X. Niu, Y. Zhu, An effective Co-promoted platinum of Co–Pt/SBA-15 catalyst for selective hydrogenation of cinnamaldehyde to cinnamyl alcohol, Catal. Lett. 146 (2016) 1535–1543.

[16] H. Shen, H. Zhao, J. Yang, J. Zhao, L. Yan, L. Chou, H. Song, A facile strategy for incorporation of PtCo alloy into UiO-66-NH_2 for cinnamaldehyde hydrogenation, Catal. Commun. 106714 (2023).

[17] V.R. Stamenkovic, B.S. Mun, M. Arenz, K.J. Mayrhofer, C.A. Lucas, G. Wang, P. N. Ross, N.M. Markovic, Trends in electrocatalysis on extended and nanoscale Pt-bimetallic alloy surfaces, Nat. Mater. 6 (3) (2007) 241–247.

[18] X. Huang, O. Akdim, M. Douthwaite, K. Wang, L. Zhao, R.J. Lewis, S. Pattisson, I. T. Daniel, P.J. Miedziak, G. Shaw, Au–Pd separation enhances bimetallic catalysis of alcohol oxidation, Nature 603 (7900) (2022) 271–275.

[19] L. Zhao, O. Akdim, X. Huang, K. Wang, M. Douthwaite, S. Pattisson, R.J. Lewis, R. Lin, B. Yao, D.J. Morgan, Insights into the effect of metal ratio on cooperative redox enhancement effects over Au-and Pd-mediated alcohol oxidation, ACS Catal. 13 (5) (2023) 2892–2903.

[20] I.T. Daniel, L. Zhao, D. Bethell, M. Douthwaite, S. Pattisson, R.J. Lewis, O. Akdim, D.J. Morgan, S. McIntosh, G.J. Hutchings, Kinetic analysis to describe Co-operative redox enhancement effects exhibited by bimetallic Au–Pd systems in aerobic oxidation, Catal. Sci. Technol. 13 (1) (2023) 47–55.

[21] H. Xin, S. Linic, Communications: Exceptions to the d-band model of chemisorption on metal surfaces: The dominant role of repulsion between adsorbate states and metal d-states, J. Chem. Phys. 132 (22) (2010) 221101.

[22] Y. Zhang, J. Su, J. Chen, C. Dai, B. Zhang, Insight into the role of iron in platinum-based bimetallic catalysts for selective hydrogenation of cinnamaldehyde, Chin. Chem. Lett. 33 (8) (2022) 3757–3761.

[23] G. Wang, H. Xin, Q. Wang, P. Wu, X. Li, Efficient liquid-phase hydrogenation of cinnamaldehyde to cinnamyl alcohol with a robust PtFe/HPZSM-5 catalyst, J. Catal. 382 (2020) 1–12.

[24] R. Prins, V.K. Pa´lfi, M. Reiher, Hydrogen spillover to nonreducible supports, J. Phys. Chem. C 116 (27) (2012) 14274–14283.

[25] A. Roucoux, J. Schulz, H. Patin, Reduced transition metal colloids: a novel family of reusable catalysts? Chem. Rev. 102 (10) (2002) 3757–3778.

[26] A.Y. Khodakov, V.L. Zholobenko, R. Bechara, D. Durand, Impact of aqueous impregnation on the long-range ordering and mesoporous structure of cobalt containing MCM-41 and SBA-15 materials, Microporous Mesoporous Mater. 79 (1) (2005) 29–39.

[27] M. Kruk, M. Jaroniec, C.H. Ko, R. Ryoo, Characterization of the porous structure of SBA-15, Chem. Mater. 12 (7) (2000) 1961–1968.

[28] E.P. Barrett, L.G. Joyner, P.P. Halenda, The Determination of Pore Volume and Area Distributions in Porous Substances. I. Computations from Nitrogen Isotherms, J. Am. Chem. Soc. 73 (1) (1951) 373–380.

[29] X. Wang, X. Liang, P. Geng, Q. Li, Recent advances in selective hydrogenation of cinnamaldehyde over supported metal-based catalysts, ACS Catal. 10 (4) (2020) 2395–2412.

[30] C. Wang, H. Daimon, S. Sun, Dumbbell-like Pt—Fe_3O_4 nanoparticles and their enhanced catalysis for oxygen reduction reaction, Nano Lett. 9 (4) (2009) 1493–1496.

[31] H. Xiao, X. Yang, M. Zhao, R. Zhang, Y. Jing, L. Zhang, Y. He, H. Wu, J. Jia, Revealing promotion of interfacial Pt–O–Fe oxygen bridge structure in PtFe/graphene synthesized by a four-electrode electrochemical system on water splitting, Int. J. Hydrogen Energy 48 (98) (2023) 38728–38741.

[32] T. Chen, Z. Shi, G. Zhang, H.C. Chan, Y. Shu, Q. Gao, Y. Tang, Molybdenum-incorporated mesoporous silica: Surface engineering toward enhanced metal–support interactions and efficient hydrogenation, Mater. Interfaces 10 (49) (2018) 42475–42483.

[33] A. Siani, O.S. Alexeev, B. Captain, G. Lafaye, P. Mar´ecot, R.D. Adams, M. D. Amiridis, Synthesis of cluster-derived PtFe/SiO_2 catalysts for the oxidation of CO, J. Catal. 255 (2) (2008) 162–179.

[34] L. DeRita, S. Dai, K. Lopez-Zepeda, N. Pham, G.W. Graham, X. Pan, P. Christopher, Catalyst architecture for stable single atom dispersion enables site-specific spectroscopic and reactivity measurements of CO adsorbed to Pt atoms, oxidized Pt clusters, and metallic Pt clusters on TiO_2, J. Am. Chem. Soc. 139 (40) (2017) 14150–14165.

[35] H. Tang, Y. Su, B. Zhang, A.F. Lee, M.A. Isaacs, K. Wilson, L. Li, Y. Ren, J. Huang, M. Haruta, Classical strong metal–support interactions between gold nanoparticles and titanium dioxide, Sci. Adv. 3 (10) (2017) e1700231.

[36] J. Miller, B. Meyers, F. Modica, G. Lane, M. Vaarkamp, D. Koningsberger, Hydrogen temperature-programmed desorption (H2-TPD) of supported platinum catalysts, J. Catal. 143 (2) (1993) 395–408.

[37] B. Zugic, S. Zhang, D.C. Bell, F. Tao, M. Flytzani-Stephanopoulos, Probing the low-temperature water–gas shift activity of alkali-promoted platinum catalysts stabilized on carbon supports, J. Am. Chem. Soc. 136 (8) (2014) 3238–3245.

[38] Y. Shi, D. Zhang, H. Huang, H. Miao, X. Wu, H. Zhao, T. Zhan, X. Chen, J. Lai, L. Wang, Mixture phases engineering of PtFe Nanofoams for efficient hydrogen evolution, Small 18 (11) (2022) 2106947.

[39] S. Xing, M. Xiong, S. Zhao, B. Zhang, Y. Qin, Z. Gao, Improving the efficiency of hydrogen spillover by an organic molecular decoration strategy for enhanced catalytic hydrogenation performance, ACS Catal. 13 (6) (2023) 4003–4011.

[40] M.P. Humbert, J.G. Chen, Correlating hydrogenation activity with binding energies of hydrogen and cyclohexene on M/Pt (111)(M=Fe Co, Ni, Cu) bimetallic surfaces, J. Catal. 257 (2) (2008) 297–306.

[41] Y. Bonita, V. Jain, F. Geng, T.P. O'Connell, N.X. Ramos, N. Rai, J.C. Hicks, Hydrogenation of cinnamaldehyde to cinnamyl alcohol with metal phosphides: Catalytic consequences of product and pyridine doping, Appl. Catal., B 277 (2020) 119272.

[42] Y. Yang, D. Rao, Y. Chen, S. Dong, B. Wang, X. Zhang, M. Wei, Selective Hydrogenation of Cinnamaldehyde over Co-Based Intermetallic Compounds Derived from Layered Double Hydroxides, ACS Catal. 8 (12) (2018) 11749–11760.

[43] Y. Dai, X. Gao, X. Chu, C. Jiang, Y. Yao, Z. Guo, C. Zhou, C. Wang, H. Wang, Y. Yang, On the role of water in selective hydrogenation of cinnamaldehyde to cinnamyl alcohol on PtFe catalysts, J. Catal. 364 (2018) 192–203.

[44] C. Rüchardt, M. Gerst, J. Ebenhoch, Uncatalyzed transfer hydrogenation and transfer hydrogenolysis: two novel types of hydrogen-transfer reactions, Angew. Chem. Int. Ed. Engl. 36 (13–14) (1997) 1406–1430.

[45] F. Wang, Z. Zhang, Catalytic transfer hydrogenation of furfural into furfuryl alcohol over magnetic γ-Fe_2O_3@HAP catalyst, ACS Sustainable Chem. Eng. 5 (1) (2017) 942–947.

[46] D. Loffreda, F. Delbecq, F. Vign´e, P. Sautet, Catalytic hydrogenation of unsaturated aldehydes on Pt (111): understanding the selectivity from first-principles calculations, Angew. Chem., Int. Ed. 44 (33) (2005) 5279–5282.

[47] L. Li, W. Wei, W. Wang, X. Wang, L. Zhang, A. Tian, Selective hydrogenation of cinnamaldehyde catalyzed by Co-doped Pt clusters: a density functional theoretical study, RSC Adv. 6 (91) (2016) 88277–88286.

[48] G. Wang, W. Gao, D. Yun, C. Xu, Z. Li, C. Xia, A reflux system to SBA-15 synthesis for selective hydrogenation of cinnamyl aldehyde, New J. Chem. 47 (2023) 12314–12319.

[49] Y. Lv, M. Han, W. Gong, D. Wang, C. Chen, G. Wang, H. Zhang, H. Zhao, Fe-Co alloyed nanoparticles catalyzing efficient hydrogenation of cinnamaldehyde to cinnamyl alcohol in water, Angew. Chem., Int. Ed. 59 (52) (2020) 23521–23526.

[50] R. Gao, L. Pan, H. Wang, Y. Yao, X. Zhang, L. Wang, J.J. Zou, Breaking trade-off between selectivity and activity of nickel-based hydrogenation catalysts by tuning both steric effect and d-band center, Adv. Sci. 6 (10) (2019) 1900054.

[51] J. Breen, R. Burch, J. Gomez-Lopez, K. Griffin, M. Hayes, Steric effects in the selective hydrogenation of cinnamaldehyde to cinnamyl alcohol using an Ir/C catalyst, Appl. Catal., A 268 (1–2) (2004) 267–274.

[52] N. Mahata, F. Gonçalves, M.F.R. Pereira, J.L. Figueiredo, Selective hydrogenation of cinnamaldehyde to cinnamyl alcohol over mesoporous carbon supported Fe and Zn promoted Pt catalyst, Appl. Catal., A 339 (2) (2008) 159–168.

[53] H. Chen, D.A. Cullen, J.Z. Larese, Highly efficient selective hydrogenation of cinnamaldehyde to cinnamyl alcohol over gold supported on zinc oxide materials, J. Phys. Chem. C 119 (52) (2015) 28885–28894.

[54] Z. Cao, J. Bu, Z. Zhong, C. Sun, Q. Zhang, J. Wang, S. Chen, X. Xie, Selective hydrogenation of cinnamaldehyde to cinnamyl alcohol over BN-supported Pt catalysts at room temperature, Appl. Catal., A 578 (2019) 105–115.

[55] Y. Dai, X. Chu, J. Gu, X. Gao, M. Xu, D. Lu, X. Wan, W. Qi, B. Zhang, Y. Yang, Water-enhanced selective hydrogenation of cinnamaldehyde to cinnamyl alcohol on RuSnB/CeO_2 catalysts, Appl. Catal., A 582 (2019) 117098.

[56] Y. Li, P.-F. Zhu, R.-X. Zhou, Selective hydrogenation of cinnamaldehyde to cinnamyl alcohol with carbon nanotubes supported Pt-Co catalysts, Appl. Surf. Sci. 254 (9) (2008) 2609–2614.

[57] Z.M. Shakor, A.A. AbdulRazak, A.A. Shuhaib, Optimization of process variables for hydrogenation of cinnamaldehyde to cinnamyl alcohol over a Pt/SiO_2 catalyst

using response surface methodology, Chem. Eng. Commun. 209 (6) (2022) 827–843.
[58] Y. Xue, R. Yao, J. Li, G. Wang, P. Wu, X. Li, Efficient Pt–FeO_x/TiO_2@SBA-15 catalysts for selective hydrogenation of cinnamaldehyde to cinnamyl alcohol, Catal. Sci. Technol. 7 (24) (2017) 6112–6123.
[59] Y. Tan, X. Liu, L. Zhang, F. Liu, A. Wang, T. Zhang, Producing of cinnamyl alcohol from cinnamaldehyde over supported gold nanocatalyst, Chin. J. Catal. 42 (3) (2021) 470–481.
[60] A. Chauhan, R. Ghalta, R. Bal, R. Srivastava, Thermocatalytic and photocatalytic chemoselective reduction of cinnamaldehyde to cinnamyl alcohol and hydrocinnamaldehyde over Ru@ZnO/CN, J. Mater. Chem. 11 (2023) 11786.